

Original Investigation

Association of a Novel *ACTA1* Mutation With a Dominant Progressive Scapulo-peroneal Myopathy in an Extended Family

Kristen Zukosky, PhD; Katherine Meilleur, PhD; Bryan J. Traynor, MD, PhD; Jahannaz Dastgir, DO; Livija Medne, MS, CGC; Marcella Devoto, PhD; James Collins, MD; Jachinta Rooney, PhD; Yaqun Zou, MD; Michele L. Yang, MD; J. Raphael Gibbs, BS; Markus Meier, PhD; Joerg Stetefeld, PhD; Richard S. Finkel, MD; Joachim Schessl, MD; Lauren Elman, MD; Kevin Felice, DO; Toby A. Ferguson, MD, PhD; Ozge Ceyhan-Birsoy, PhD; Alan H. Beggs, PhD; Gihan Tennekoon, MD; Janel O. Johnson, PhD; Carsten G. Bönnemann, MD

IMPORTANCE New genomic strategies can now be applied to identify a diagnosis in patients and families with previously undiagnosed rare genetic conditions. The large family evaluated in the present study was described in 1966 and now expands the phenotype of a known neuromuscular gene.

OBJECTIVE To determine the genetic cause of a slowly progressive, autosomal dominant, scapulo-peroneal neuromuscular disorder by using linkage and exome sequencing.

DESIGN, SETTING, AND PARTICIPANTS Fourteen affected individuals in a 6-generation family with a progressive scapulo-peroneal disorder were evaluated. Participants were examined at pediatric, neuromuscular, and research clinics from March 1, 2005, to May 31, 2014. Exome and linkage were performed in genetics laboratories of research institutions.


MAIN OUTCOMES AND MEASURES Examination and evaluation by magnetic resonance imaging, ultrasonography, electrodiagnostic studies, and muscle biopsies (n = 3). Genetic analysis included linkage analysis (n = 17) with exome sequencing (n = 7).

RESULTS Clinical findings included progressive muscle weakness in an initially scapulo-peroneal and distal distribution, including wrist extensor weakness, finger and foot drop, scapular winging, mild facial weakness, Achilles tendon contractures, and diminished or absent deep tendon reflexes. Both age at onset and progression of the disease showed clinical variability within the family. Muscle biopsy specimens demonstrated type I fiber atrophy and trabeculated fibers without nemaline rods. Analysis of exome sequences within the linkage region (4.8 megabases) revealed missense mutation c.591C>A p.Glu197Asp in a highly conserved residue in exon 4 of *ACTA1*. The mutation cosegregated with disease in all tested individuals and was not present in unaffected individuals.

CONCLUSIONS AND RELEVANCE This family defines a new scapulo-peroneal phenotype associated with an *ACTA1* mutation. A highly conserved protein, *ACTA1* is implicated in multiple muscle diseases, including nemaline myopathy, actin aggregate myopathy, fiber-type disproportion, and rod-core myopathy. To our knowledge, mutations in Glu197 have not been reported previously. This residue is highly conserved and located in an exposed position in the protein; the mutation affects the intermolecular and intramolecular electrostatic interactions as shown by structural modeling. The mutation in this residue does not appear to lead to rod formation or actin accumulation in vitro or in vivo, suggesting a different molecular mechanism from that of other *ACTA1* diseases.

JAMA Neurol. 2015;72(6):689-698. doi:10.1001/jamaneurol.2015.37
Published online May 4, 2015. Corrected on July 9, 2015.

 Video at jamaneurology.com

 Supplemental content at jamaneurology.com

Author Affiliations: Author affiliations are listed at the end of this article.

Corresponding Author: Carsten G. Bönnemann, MD, National Institute of Neurological Disorders and Stroke, National Institutes of Health, 35 Convent Dr, MSC 3705, Room 2A116, Bethesda, MD 20814 (carsten.bonnemann@nih.gov).

Scapuloperoneal syndromes are a highly heterogeneous group of skeletal muscle and nerve disorders associated with weakness and wasting of scapular fixators and anterior distal leg muscles.¹ This pattern of weakness is seen in certain myopathies, including Emery-Dreifuss muscular dystrophy, hyaline body myopathy, and reducing body myopathy.¹ Neurogenic disorders can also be present in a scapuloperoneal distribution as seen with some *TRPV4* (OMIM 605427) mutations.²

In 1966, Armstrong and colleagues³ reported on 2 individuals from a family with a dominantly inherited phenotype of early onset, predominantly scapuloperoneal muscle weakness. The disorder was classified as proximal spinal muscular atrophy on the basis of biopsy and electromyographic findings interpreted as neurogenic changes. The family returned for further evaluation of 14 patients from an expanded 6-generation pedigree with 33 known affected individuals who presented with scapulohumeroperoneal weakness as well as distal hand and mild facial involvement. The disease was progressive but of highly variable severity in the family. Linkage analysis combined with exome sequencing revealed a novel mutation in *ACTA1* (OMIM 102610) in a highly conserved residue, which cosegregated with the clinical phenotype.

The actinopathies are caused by mutations in skeletal muscle actin encoded by *ACTA1*. They cover a heterogeneous spectrum of clinical severity and histomorphologic expression,⁴⁻⁶ including nemaline myopathy, intranuclear rod myopathy, rod-core myopathy, actin aggregation, zebra bodies, and fiber-type disproportion.^{5,7} The *ACTA1*-related scapuloperoneal myopathy without nemaline rods or actin accumulations reported in this family does not belong to any of the hitherto recognized clinicopathologic actinopathies and thus expands the phenotypic range of actinopathies.

Methods

In this observational study, we examined 14 affected individuals from a 6-generation pedigree. The study was conducted from March 1, 2005, to May 31, 2014. The institutional review board of the National Institute of Neurological Disorders and Stroke approved the study. Written informed consent was obtained from all participants, who received financial compensation. Patient consent-to-disclose forms included consent for publication and were obtained for all photos and videos.

Neurologic Examination

A comprehensive neurologic examination was performed. A summary of the findings of the examination is presented in the Table.

Muscle Biopsy and Immunocytochemistry

Histochemical stains, including hematoxylin-eosin, Gomori-trichrome, and nicotinamide adenine dinucleotide tetrazolium reductase, were performed on 9- μ m frozen muscle samples. For immunohistochemical analysis, sections and cells were fixed in 4% para-formaldehyde, blocked in 0.1% Tx-100/

10% fetal bovine serum/phosphate-buffered saline, incubated with primary antibodies (anti- α sarcomeric actin clone 5C5, Sigma; LamaA2 Leica Biosystems; MHC-s Leica, MHC-f Leica, and NCL- α -actinin [recognizing α -actinin 1] Leica; nNOS Life Technologies) overnight at 4°C; incubated with AlexaFlour secondary antibodies (goat antimouse 488, goat antirabbit 596); and mounted with Fluoromount-G mounting solution (eBioscience Inc). Images were acquired on an epifluorescent microscope (Nikon Eclipse Ti).

Muscle Ultrasonography

Skeletal muscle ultrasonography was performed using an L12-5 linear transducer at 12 MHz on a Philips iu22 system. Muscles of the thigh, calf, and proximal arm were imaged.

Motor Unit Number Estimation

The estimated number of motor units innervating hypothenar muscles (motor unit number estimation [MUNE]) was based on published⁸ multiple-point stimulation techniques (Teca Synergy N-EP machine; Cardinal Health). The MUNE value was calculated by dividing the maximum compound muscle action potential negative peak amplitude by the mean surface motor unit potential negative peak amplitude. In addition, conventional nerve conduction studies and electromyography (Nicolet) were performed on one patient (IV-25).

Linkage Analysis

Genotyping was performed using Illumina Linkage IV Panel, which includes 5861 informative single-nucleotide polymorphism (SNP) markers distributed evenly across the human genome at an average distance of 0.64 centimorgans. The SNP data were analyzed using Merlin⁹ linkage software, version 1.1.2, assuming a fully penetrant dominant model of disease transmission.

Exome Sequencing

The DNA from affected individuals IV-23, IV-25, V-6, V-8, V-10, V-11, and VI-9 was enriched (SureSelect Exome target enrichment, version 1.0; Agilent Technologies). The enriched DNA was paired-end sequenced (Genome Analyzer IIX; Illumina). Sequence alignment and variant calling were performed using Burrows-Wheeler Aligner,¹⁰ the Genome Analysis Toolkit,^{11,12} and Picard (<http://picard.sourceforge.net/index.shtml>). The Burrows-Wheeler Aligner was used to align the paired-end sequence against the reference human genome (UCSC hg18). The Genome Analysis Toolkit was used to recalibrate quality scores, perform local realignments around insertions and deletions, identify variants, and call genotypes. Polymerase chain reaction duplicates were removed using Picard prior to variant calling with the Genome Analysis Toolkit. Based on the hypothesis that the mutation underlying this rare familial disease was not present in the general population, SNPs identified in the 1000 Genomes project (<http://www.1000genomes.org/>) or in dbSNP (<http://www.ncbi.nlm.nih.gov/projects/SNP>, Build 131) were removed. We excluded variants that were not shared by all patients. Next, synonymous changes were identified and filtered from the variant list using SIFT, version 4.0 (<http://sift.jcvi.org/>).

Table. Clinical Examination Findings^a

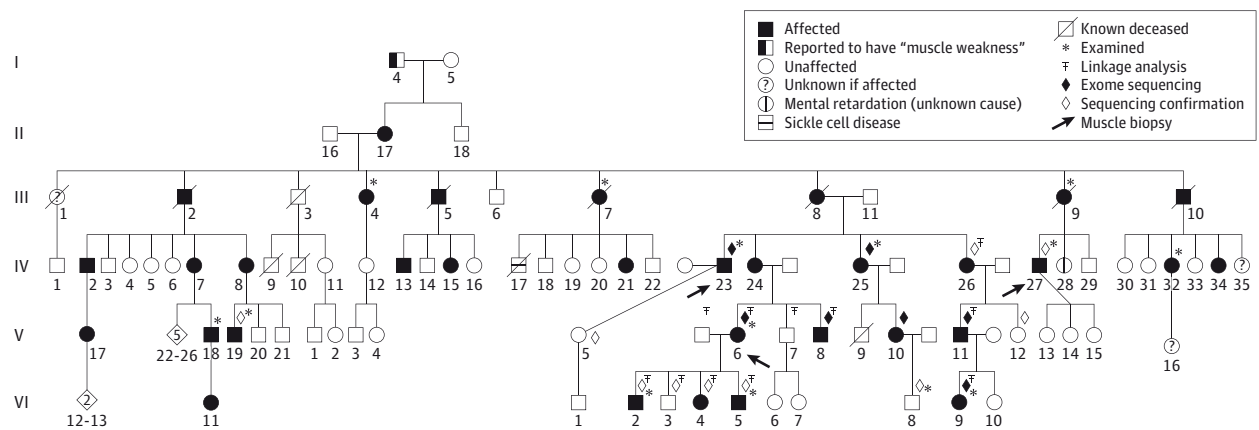
Characteristic	Patient											
	III-4	III-7	III-9	IV-23	IV-25	IV-27	IV-32	V-6	V-18	V-19	VI-2	VI-5
Cranial Nerves												
Ptosis	NR	-	-	NR	NR	-	NR	+/-	NR	-	+/-	-
Facial weakness												
Extraocular	-	-	-	NR	-	-	-	-	-	-	-	-
Periocular	-	-	-	+	+	-	-	+	+	-	+	+
Transverse smile	+	-	-	+	+	-	+	+	+	-	+	-
Neck weakness												
Flexor	+++	++	++	+++	+	+	+	+	+	+	++	+
Extensor	NR	+	+	NR	-	-	NR	-	NR	+	+/-	+
Upper Extremity Weakness Pattern												
Proximal muscle groups												
Scapular winging	NR	-	-	+	+	++	+/-	+/-	+	+	+	+
Latissimus dorsi	NR	NR	NR	0	NR	NR	+	-	+	NR	0	+
Rhomboids	NR	NR	NR	++	-	NR	NR	-	NR	NR	+	NR
Deltoids	+++	+++	0	0	+	+	+	+	+++	+	0	+
Biceps	+++	++	+++	+++	-	+	+/-	-	+++	+	+++	+
Triceps	++	+	++	+++	-	+/-	+/-	-	+	+	++	+
Distal muscle groups												
Wrist extension	NR	++	+	+++	-	+/-	+	+	++	+	++	+
Wrist flexion	NR	++	+	+++	-	+/-	NR	+	++	+	++	+
Finger abduction	+++	NR	NR	+++	++	NR	+	+	+++	NR	+++	+
Finger extension	+++	++	+	+++	+	++	+	++	NR	++	++	+
Grip	++	++	+	+	+	++	+	-	+	++	+	+
Thumb adduction	NR	NR	NR	+	+	+	NR	+	NR	+	++	NR
Thumb abduction	+++	NR	NR	+++	++	+	NR	+++	+++	+	+++	NR
Trunk												
Weakness	NR	NR	NR	-	-	NR	NR	-	NR	NR	-	-
Scoliosis	NR	NR	NR	-	-	NR	NR	-	NR	NR	-	-
Lower Extremity Weakness Pattern												
Proximal												
Hip flexor	NR	++	+++	+	+	+/-	+	+	+	+	+	+
Hip extensor	NR	NR	NR	+	-	NR	NR	-	NR	+	NR	+/-
Knee flexor	++	++	+++	++	-	+/-	+	-	+/-	+	+/-	+
Knee extensor	+++	++	+++	+++	+++	+/-	-	-	-	+	-	+/-
Leg abductor	+	+	+	+/-	-	+	+/-	+	-	+	+	+
Leg adductor	+	+	+	+	+/-	+	NR	+	-	+	+/-	+/-
Distal												
Dorsiflexion	+++	0	0	0	++	++	+	+	+++	++	+++	++
Plantar flexion	+	++	+	+	+	+/-	+/-	-	+	+	-	-
Foot eversion	+++	+++	+++	0	++	++	+	+	+++	+	+++	++
Foot inversion	+	++	++	-	+	+	+/-	-	+	+	+	+/-
First toe dorsiflex	NR	NR	NR	+++	++	NR	NR	+	NR	NR	NR	NR
Mobility												
Gait												
Ambulation	NAmb	NAmb	NAmb	Short distance	+	+	+	+	+	NR	+	+
Foot drop	-	NR	NR	+	+	NR	+	-	+	+	+	+
Hyperextended at knees	NR	NR	NR	+	+	NR	NR	-	NR	+	NR	-
Wheelchair	+	+	+	+	NR	NR	NR	NR	NR	-	-	NR
Creatine kinase, U/L	NR	NR	NR	105	69	46	NR	103	NR	NR	316	NR

Abbreviations: NAmb, nonambulatory; NR, not recorded.

SI conversion factor: To convert creatine kinase to microkatal per liter, multiply by 0.0167.

^a Findings are presented as -, negative or normal strength; +/-, minimally affected; +, mildly affected; ++, moderately affected; +++, severely affected; and 0, no movement.

Figure 1. Expanded 6-Generation Pedigree



An extensive pedigree of the family with the novel *ACTA1* mutation depicting affected members in each generation, with a total of 33 known affected individuals. Circles indicate female; squares, male. The numbers within triangles indicate the number of additional children (not all unaffected children were drawn out individually).

Molecular Modeling

The high-resolution crystal structure of human actin (pdb-code: 3DAW; sequence identity: 100%) was used as a modeling template.¹³ The implemented single-point mutation of glutamic acid (Glu)197 to aspartic acid (Asp)197 was subject to gradient energy minimization in the Crystallography and NMR system.¹⁴ The lowest energy structures of the single-point mutant version were subject to 500 cycles of unrestrained Powell minimization. Harmonic restraints were imposed on the target molecule (2 kcal/mol Å²) with increased weight (25 kcal/mol Å²). Protein structure and model assessment tools were used to verify the quality of the modeled structure.

Transfection and Western Blotting

Cos-7 cells were transfected with WT-eGFP, Asp286Gly-eGFP, and Asp197Glu-eGFP constructs (Lipofectamine; Invitrogen). Immunocytochemical analysis was performed as described above. For the Western blot, primary antibody to α 1 actin (Sigma) and secondary goat antimouse IgG-horseradish peroxidase was used. Proteins were resolved by electrophoresis on a 4% to 12% gradient Bis-Tris polyacrylamide gel and blotted according to a standard protocol.

Zebrafish Studies

Wild-type and Glu197Asp human *ACTA1* genes were cloned into pCSDest vector (Addgene) as described.¹⁵ Plasmids were linearized with restriction enzyme *NotI*, and RNA was transcribed using a kit (SP6 mMessage Machine kit; Ambion). One-cell stage embryos were injected with 200 pg and 400 pg of RNA, and muscle was analyzed as described previously¹⁶ using Acti-stain 670 (Cytoskeleton Inc) and antimyosin heavy chain antibody (F59; Santa Cruz Biotech).

Results

Clinical Findings

We examined 14 patients from an expanded 6-generation pedigree, in which 33 individuals are known to be affected (Figure 1).

Muscle weakness was noted in both the lower and upper extremities. The lower extremities exhibited an initial pattern of distal, more than proximal, involvement with early foot drop, but proximal involvement became more pronounced with age. The overall distribution of muscle involvement was scapulo-humeral-peroneal with additional hand involvement. Early scapular winging (Figure 2, patients VI-2 and VI-5), muscle atrophy of the thenar and deltoid muscles (Figure 2, patient V-6), and mild lower facial weakness (Figure 2, patient IV-23) were typical. Hand involvement was particularly notable, including wrist and finger drop (in particular, digits 3-5). Affected individuals developed contractures of the Achilles tendon, elbow, and shoulder. Deep tendon reflexes were diminished or absent. Phenotypic variability was evident in that more severely affected patients presented with hypotonia, foot eversion, and dorsiflexion weakness from infancy (Figure 2, patient V-6), with a “notch” in the shoulder muscle noted by their parents. Running in childhood was awkward, followed by progressive weakness resulting in loss of independent ambulation and development of scoliosis in the fifth or sixth decade of life (III-4, III-7, and III-9). In the most severely affected patients (IV-23 and VI-2), marked weakness and atrophy were especially apparent in the upper extremities, with no remaining antigravity strength in the proximal and shoulder muscles, even while still ambulant. For example, at age 15 years, this was evident in patient VI-2 (Video 1 and Video 2), and patient IV-23 was initially able to walk short distances, but the condition progressed to loss of ambulation. One of the youngest patients (VI-5), examined at age 9 years, showed less severe weakness in a similar pattern, consistent with the slowly progressive nature of the disease. Other affected individuals did not note weakness until early adulthood. Detailed findings are listed in the Table.

Muscle Imaging

On muscle ultrasonography, findings were variable, although atrophy was apparent in all patients. Advanced muscle involvement with uniform increase in echogenicity in patient IV-23 is shown in eFigure 1 in the Supplement. In patient V-6,

Figure 2. Clinical Photographs



Patient VI-2 shows generalized muscle atrophy and scapular winging. Patient VI-5 demonstrates early scapular winging. Patient IV-23 shows mild facial weakness, wrist and finger extension weakness with wrist and finger drop, and pronounced deltoid atrophy. Patient V-6 demonstrates hypothenar atrophy but full finger extension as well as foot drop and high arches.

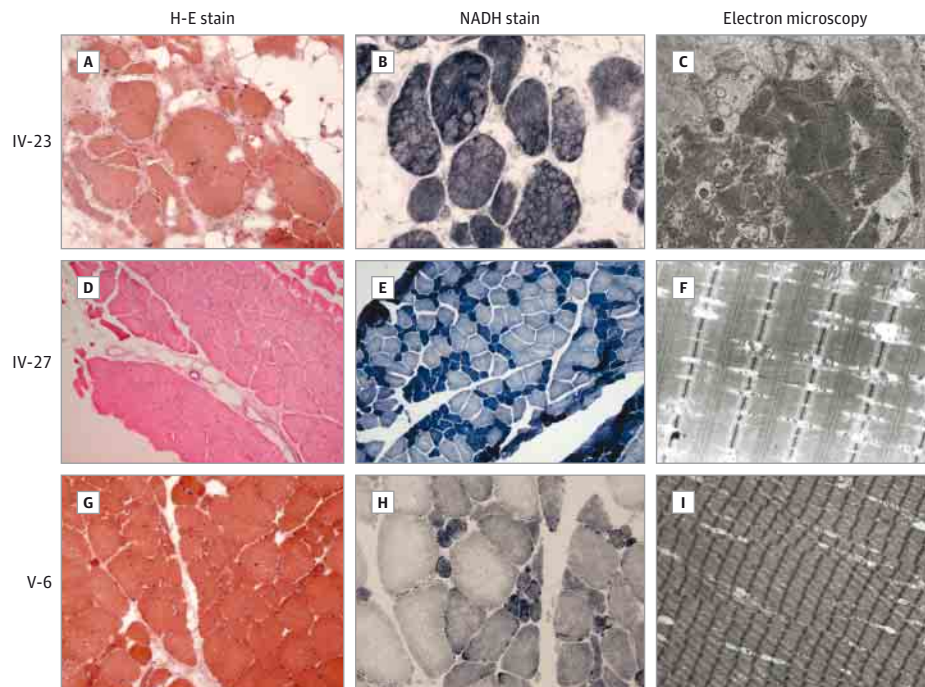
a mixed granular and streaklike pattern was observed (eFigure 1 in the Supplement). Muscle magnetic resonance imaging was performed on patients IV-23 and V-6. Patient IV-23 showed marked atrophy, as well as significant fatty replacement of the quadriceps and, in particular, of the vastus intermedius and the rectus femoris; the hamstring muscles also demonstrated severe involvement with some notable sparing of parts of the semitendinosus and adductor longus muscles (eFigure 1 in the Supplement). In contrast, patient V-6 was more mildly affected, with minimal involvement of the sartorius, biceps femoris, and vastus lateralis (eFigure 1 in the Supplement).

Histopathologic Findings

Muscle biopsies from patients IV-23, IV-27, and V-6 (Figure 3) demonstrated variability of histologic findings, suggesting

progression with age. The muscle in patient IV-23 was initially biopsied in childhood and, as reported in the original article,³ showed groups of atrophic fibers. The more recent muscle biopsy in this patient, obtained from the tibialis anterior, demonstrated end-stage muscle with marked degenerative features including dramatic variability in fiber size (with atrophic and hypertrophic fibers), greatly increased internalization of nuclei, and fatty infiltration. On nicotinamide adenine dinucleotide stain, frequent trabeculated or lobulated fibers were noted (Figure 3). In contrast, muscle biopsies from the less affected patients (IV-27 and V-6) indicated milder changes, although groups of atrophic fibers of type I were present, consistent with fiber-type disproportion. None of the muscle biopsies revealed nemaline rods on modified Gomori-trichrome stain or electron microscopy or actin aggregates by

Figure 3. Muscle Biopsy Histology



Histology in patients IV-23 (A, B, and C), IV-27 (D, E, and F), and V-6 (G, H, and I). In patient IV-23 (tibialis anterior), hematoxylin-eosin (H-E) stain demonstrated muscle with great fiber size variability, centralized nuclei, and myofiber degeneration, as well as fatty and connective tissue infiltration (A); the nicotinamide adenine dinucleotide tetrazolium reductase (NADH) stain revealed the presence of trabeculated fibers (B). The biopsy from patient IV-27 (vastus lateralis) showed fiber size variability with groups of atrophic fibers (D)

that, on NADH stain, were dark and thus were type I. Patient V-6's biopsy (biceps) revealed variability in fiber size with groups of atrophic fibers and some degree of central nucleation (G); on NADH staining, the small fibers were dark, again indicating fiber type I atrophy (H). Ultrastructural examination in patient IV-23 demonstrated disrupted myofibrils in severely atrophic fibers but no rod formation (C), whereas patients IV-27 and V-6 had normally aligned Z-discs and no evidence of rod formation (F and I).

immunohistochemistry or electron microscopy (Figure 3, eFigure 2 in the Supplement). The nNOS staining was robust in the atrophic fibers, arguing against denervation as a cause for the atrophy (eFigure 3 in the Supplement).

MUNE Results

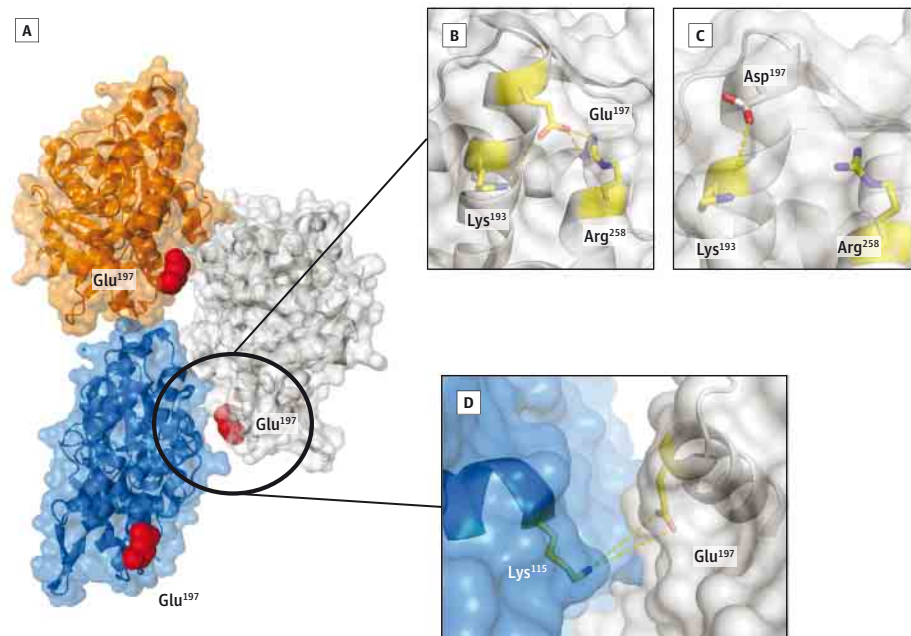
For patient VI-2, the compound muscle action potential amplitude of the right ulnar nerve was 7005 μ V, and the mean surface motor unit potential was 119 μ V. The MUNE of the right ulnar nerve was 59. For unaffected relative VI-8, the compound muscle action potential amplitude of the right ulnar nerve was 10 773 μ V, and mean surface motor unit potential was 57 μ V. The MUNE of the right ulnar nerve was 189. Results of nerve conduction studies of the right arm and leg of one later affected family member (IV-25) were normal. Electromyography of the right side demonstrated large polyphasic motor units with delayed recruitment, especially in weaker muscles (knee extensors), but occasional small-amplitude, polyphasic motor units were also observed in less affected muscles (deltoid). No abnormal spontaneous activity was observed.

Genetic Analysis

Samples of DNA were collected from 19 individuals. Linkage analysis in 17 family members (Linkage IV Panel, Illumina;

and Merlin software) identified a 4.8-megabase region (rs1340867 to rs1043909, Chr1:225,611,595-230,417,121) on chromosome 1q42.12-q42.13 with a logarithm (base 10) of odds score of greater than 2 and a maximum logarithm (base 10) of odds score of 3.651, containing 49 genes with open reading frames in this single significant linkage region (eTable in the Supplement). Whole-exome sequencing was performed in 7 individuals, with the analysis focused on the linkage region. There were 481 baits to cover the region; 427 of these baits had a coverage of a mean read depth of 10 or more in at least 3 of the 7 affected individuals sequenced, resulting in an estimated coverage at an average read depth of 10 or more in the region at 88.77% for at least 3 of the sequenced individuals (mean read depth, 84.19% for all 7 participants). The average read depth for all baits in the region in all 7 individuals was 143. Variant analysis in the linkage region detected only 1 nonsynonymous variant in all 7 affected individuals: c.591C>A p.Glu197Asp in exon 4 of *ACTA1*. This variant is not a recorded variant in dbSNP and is not seen in the 60 706 exome ExAC database at the Broad Institute (<http://exac.broadinstitute.org>). The mutation was confirmed in the heterozygous state by Sanger sequencing (eFigure 4 in the Supplement) and was shown to cosegregate with the phenotype in the extended pedigree (n = 19) (Figure 1).

Figure 4. Molecular Implication of the E197D Mutant on F-Actin Assembly



A, Overall view of the trimeric minimal F-actin filament. The lateral actin monomer is gray, the longitudinal monomer is shown in blue, and brown indicates a third actin molecule because that is how they interact. The glutamic acid (Glu)197 residue is highlighted in red spheres. B, Detailed view of the intramolecular interaction mediated by Glu197. First, an intrahelical i to $i+4$ salt bridge is formed along the helical dipole with the side chain of lysine (Lys)193. Second, the remaining part of the carboxylate moiety of Glu197 is oriented toward arginine (Arg)258, forming a salt bridge. C, The replacement of Glu197 by an aspartate side chain causes a severe effect on the radius of action

residue 197. In the aspartic acid (Asp)197 version of actin, the interaction with Arg258 is disrupted and Asp197 is just forming the intrahelical interaction with Lys193. D, Glu197 also mediates an intermolecular interaction along the helical element of the F-actin filament. The side chain forms an electrostatic interaction with the basic Lys115 of the neighboring longitudinal subunit. In the case of the Glu197Asp mutant, this interaction is disrupted (not shown). In B, C, and D, red indicates the negatively charged side chains, blue represents the positively charged side chains, and greenish yellow shows the position of the amino acid.

Structural Modeling and Interpretation

Monomeric actin can oligomerize into double-stranded F-actin trimers. In the trimer, which represents a minimal F-actin filament seed, Glu197 is a critical semisurface-exposed residue that is involved in 2 major interaction sites (Figure 4). The glutamic moiety forms a network of 2 short-range intramolecular interactions mediating a spatial bridging of lysine (Lys)193 and arginine (Arg)258 (Figure 4). However, Glu197 is in medium-range distance to the basic charged side chain of Lys115, forming an electrostatic interaction between 2 neighboring actin subunits at the fast-growing barbed end of the F-actin filament (Figure 4C). Our modeling approach revealed a significant effect of the single-point mutation Glu197Asp. Shortening of the acidic side chain by a single methylene unit causes a seriously diminished radius of action (Figure 4C), with dramatic effects on both intramolecular and intermolecular interactions. Asp197 is not able to establish the intermolecular salt bridge with Lys115 from the longitudinal subunit. In addition, Arg258 is not engaged in an electrostatic interaction with Asp197. Instead, the carboxylic moiety of Asp197 is forming a singular salt bridge with Lys193.

Functional Analysis

To determine whether the Glu197Asp mutation can lead to rod formation, Cos-7 cells were transfected with WT-eGFP,

Asp286Gly-eGFP, and Glu197Asp-eGFP constructs. The Asp286Gly-eGFP construct was used as a positive disease control that was known to form nemaline rods after transfection in culture; a mock transfection was used as a negative control. Neither immunostaining nor Western blot showed any significant changes in actin localization between the Glu197Asp-eGFP construct and WT-eGFP, whereas the positive disease control resulted in rod formation as expected and previously reported¹⁷ (eFigure 5 in the Supplement). However, no intranuclear rods were seen. The constructs were also transfected into HEK, NIH3T3, and C2C12 cells, none of which showed a phenotype of rod formation or abnormalities of the actin skeleton at 24, 48, 72, 96, or 120 hours (eFigure 6 in the Supplement). In addition, zebrafish injected with RNA encoding either wild type or Glu197Asp human ACTA1 displayed no abnormalities in their morphology or muscle histology up to 6 days after fertilization, including no actin accumulations or sarcomeric disorganization (eFigure 7 in the Supplement).

Discussion

In this study, we identified a novel variant in ACTA1 associated with scapuloperoneal myopathy in a multigenerational family with a phenotype different from that of previously

recognized actinopathies. To our knowledge, this family also represents the largest single actinopathy pedigree recognized to date. Notably, the family had been first described³ in 1966 as having a form of proximal or scapuloperoneal spinal muscular atrophy. We reevaluated 14 of the 33 patients from 4 of 6 generations known to be affected.

The core clinical phenotype, present in affected family members, manifested as early as infancy with a predominantly scapuloperoneal, but more precisely scapulo-humeral-peroneal-distal, distribution of weakness with scapular winging. Over time, the muscle weakness progressed to other proximal muscle groups. Shared clinical characteristics included mild lower facial weakness, foot drop due to foot eversion and dorsiflexion weakness, finger drop of digits 3 to 5, and selective muscle atrophy. We recognized significant variability between family members regarding age of onset and severity. Some patients had onset in early childhood and were severely affected by their teenage years (VI-2); others did not experience an onset of weakness until their teenage years or adulthood (V-6 and IV-32). Some of the patients were significantly more affected in the upper limbs (VI-6 and IV-23); others were more equally affected in their lower limbs and lost ambulation (IV-25). This variability does not seem to segregate with sex or among distinct branches in the family tree but suggests that genetic modifiers may play a role. There was no evidence for cardiac, early respiratory, or extraocular muscle involvement.

The initial classification¹ as a proximal spinal muscular atrophylike phenotype in 1966 was based on electrophysiologic and biopsy data, suggesting the presence of denervation. Loss of motor units due to nonfunctional neuromuscular junctions may account for the reduced MUNE values and apparent denervation demonstrated on electrophysiologic testing. In support of this interpretation, other investigators^{18,19} have observed loss of motor units in muscular dystrophies and chronic myopathies with mixed myopathic and neurogenic features on electromyography. Thus, we suspect the striking muscle fiber atrophy observed in this family accounts for the “pseudoneurogenic” findings on biopsy and electrophysiologic testing. The fact that we found that atrophic fibers were not nNOS deficient also argues in favor of a myopathic rather than neurogenic origin.

We applied a combined linkage/whole-exome sequencing approach, which is particularly powerful in large multiplex families such as this one. This strategy resulted in a significantly linked 4.8-megabase region on chromosome 1, in which only the variant p.Glu197Asp in *ACTA1* qualified as pathogenic. This variant segregated perfectly with disease manifestation throughout the extended family.

Because *ACTA1* is one of the most highly conserved genes in muscle, it does not generally tolerate missense changes. Most amino acid sequence-changing variants recognized in *ACTA1* have thus far been pathogenic with primarily a dominant mode of action, while most recognized polymorphic sequence variants in the gene are synonymous on the amino acid level.²⁰

Compared with the known clinicopathologic entities within the actinopathies, the family reported here is differ-

ent clinically as well as morphologically. The *ACTA1*-related myopathies (actinopathies)²¹ in general tend toward more severe clinical phenotypes manifesting at birth, including arthrogryposis²² and significant hypotonia,^{23,24} as well as early respiratory involvement.²⁵ In some cases, milder clinical presentations have been recognized in individuals with nonprogressive, mild skeletal muscle weakness but significant diaphragmatic²⁶ respiratory involvement, with nemaline rods evident on biopsy.²⁶ Unusual clinical features in our family include the scapulo-humeral-peroneal-distal distribution with striking upper extremity predilection in some individuals, progressive but variable course of the disease, and sparing of respiratory muscles until very late in the disease.

Typical findings on muscle biopsy vary among actinopathies, and previous reports²⁶⁻²⁸ include cytoplasmic and/or intranuclear nemaline rods, actin aggregates, fiber-type disproportion, and zebra body formation. Muscle biopsy specimens in this family notably showed no nemaline rods, even in advanced stages of the disease. Although the fiber-type disproportion observed in our family has been observed²² in *ACTA1* mutations as part of the possible histologic spectrum, lobulated or trabeculated fibers, as seen in the more advanced biopsy, have not been reported in patients with actinopathy. However, this cytoarchitectonic abnormality is not specific in itself and has been described in a few other cases of muscular diseases.²⁹⁻³¹

Mutations in the *ACTA1* residue Glu197 have not been previously reported,⁵ but mutations in adjacent residues have been shown to be pathogenic: Thr196Pro and Arg198Cys both result in a severe nemaline myopathy.³² Evaluation of the pathogenicity of Glu197Asp by PolyPhen-2 and SIFT (amino acid change prediction website: <http://sift.jcvi.org>) predicts a relatively mild change consistent with the comparatively less severe and unusual phenotype displayed in this family. Localization of this residue on the 3-dimensional model of actin shows it is located on the exterior surface of the protein. Further modeling of the mutation reveals it to significantly affect both short-range intramolecular interactions with Lys193 and Arg258 and medium-range intermolecular electrostatic interactions with Lys115 on neighboring actin subunits. The interacting Arg258 (labeled in reference as Arg256) has been shown²¹ to be involved in a severe nemaline myopathy.

To further study the functional consequences of the mutation, mutation constructs were tested in various cell types. In contrast to the nemaline rod formation seen after transfection of a typical nemaline myopathy-associated mutation,³³ no apparent change in actin cytoarchitecture or rod formation was observed with Glu197Asp, nor were any effects on the protein level noted. In addition, injection of Glu197Asp RNA into zebrafish embryos did not result in whole-mount morphologic abnormalities. It is therefore possible that the Glu197Asp mutation may instead reflect a fundamentally different pathogenesis, such as changes in interaction or force generation, actin filament stability, or differences in the directionality of actin filament growth, for which further investigation is necessary and underway.

Conclusions

We define a novel *ACTA1* mutation in a highly conserved residue as the only significant change in a complete genetic analysis of this family. We thus identify this disorder as a new actinopathy with slowly progressive clinical manifestations, including a scapulo-humeral-peroneal-distal distribution of muscle weakness and wide intrafamilial phenotypic

variability in the age of onset and severity. In addition, no rods or inclusions were visible on muscle biopsy. Identification of *ACTA1* mutations in additional patients with this unusual clinical-morphologic presentation will further improve the understanding of the clinical, morphologic, and genetic spectrum of this phenotype. Further studies are planned to identify possible disease modifiers, which would account for the variability among affected individuals.

ARTICLE INFORMATION

Accepted for Publication: January 12, 2015.

Published Online: May 4, 2015.
doi:10.1001/jamaneurol.2015.37.

Author Affiliations: National Institute of Neurological Disorders and Stroke, National Institutes of Health, Bethesda, Maryland (Zukosky, Rooney, Zou, Bönnemann); National Institute of Nursing Research, National Institutes of Health, Bethesda, Maryland (Meilleur); Neuromuscular Diseases Research Section, Laboratory of Neurogenetics, Porter Neuroscience Research Center, National Institute on Aging, National Institutes of Health, Bethesda, Maryland (Traynor, Johnson); Division of Child Neurology, Columbia University Medical Center, New York, New York (Dastgir); Department of Neurology, The Children's Hospital of Philadelphia, Philadelphia, Pennsylvania (Medne, Tennekoon); Department of Pediatrics, Perelman School of Medicine, University of Pennsylvania, Philadelphia (Devoto); Department of Biostatistics and Epidemiology, Perelman School of Medicine, University of Pennsylvania, Philadelphia (Devoto); Department of Molecular Medicine, University La Sapienza, Rome, Italy (Devoto); Division of Genetics, The Children's Hospital of Philadelphia, Philadelphia, Pennsylvania (Devoto); Department of Neurology, Cincinnati Children's Hospital Medical Center, Cincinnati, Ohio (Collins); Research Center for Genetic Medicine, Children's National Medical Center, Washington, DC (Rooney); Department of Pediatrics and Neurology, Children's Hospital Colorado, Aurora (Yang); Computational Biology Core, Laboratory of Neurogenetics, Porter Neuroscience Research Center, National Institute on Aging, National Institutes of Health, Bethesda, Maryland (Gibbs); Department of Chemistry, Microbiology, Biochemistry, and Medical Genetics, University of Manitoba, Winnipeg, Manitoba, Canada (Meier, Stetefeld); Department of Pediatrics, Nemours Children's Hospital, Orlando, Florida (Finkel); Department of Neurology, Friedrich-Baur Institute, Ludwig-Maximilians University of Munich, Munich, Germany (Schessler); Department of Neurology, University of Pennsylvania, Philadelphia (Elman); Department of Neuromuscular Medicine, Hospital for Special Care, New Britain, Connecticut (Felice); Shriners Pediatric Research Center, Department of Neurology, Temple University, Philadelphia, Pennsylvania (Ferguson); The Manton Center for Orphan Disease Research, Division of Genetics and Genomics, Boston Children's Hospital, Harvard Medical School, Boston, Massachusetts (Ceyhan-Birsoy, Beggs).

Author Contributions: Dr Bönnemann had full access to all the data in the study and takes responsibility for the integrity of the data and the accuracy of the data analysis.

Study concept and design: Zukosky, Meilleur, Traynor, Rooney, Bönnemann.

Acquisition, analysis, or interpretation of data: All authors.

Drafting of the manuscript: Zukosky, Meilleur, Johnson, Bönnemann.

Critical revision of the manuscript for important intellectual content: Meilleur, Traynor, Dastgir, Medne, Devoto, Collins, Rooney, Zou, Yang, Gibbs, Meier, Stetefeld, Finkel, Schessler, Elman, Felice, Ferguson, Ceyhan-Birsoy, Beggs, Tennekoon, Johnson, Bönnemann.

Statistical analysis: Devoto, Ceyhan-Birsoy.

Obtained funding: Traynor, Meier, Beggs, Bönnemann.

Administrative, technical, or material support: Collins, Rooney, Zou, Yang, Gibbs, Schessler, Felice, Ferguson, Tennekoon, Bönnemann.

Study supervision: Traynor, Meier, Beggs, Bönnemann.

Conflict of Interest Disclosures: Ms Medne is a consultant for BioReference Laboratories, Elmwood Park, NJ. Dr Ferguson is a full-time employee of Biogen Idec and owns stock in Biogen Idec. No other disclosures were reported.

Funding/Support: This study was funded in part by the Division of Intramural Research of the National Institutes of Neurological Disorders and Stroke and the National Institute on Aging. This work was supported in part by National Institutes of Health grants R01HD075802 and R01AR044345, the Muscular Dystrophy Association (United States) MDA201302, the AUism Charitable Foundation, and A Foundation Building Strength (Dr Beggs). Dr Stetefeld is a Canada Research Chair in Structural Biology, and this research was funded by the Canadian Institute of Health Research/Manitoba Health Research Council Regional Partnership Program Grant RPA-109759. Dr Ceyhan-Birsoy was supported by a Dubai-Harvard Foundation for Medical Research postdoctoral fellowship and a Schlumberger Foundation Faculty for the Future grant.

Role of the Funder/Sponsor: The funding organizations had no role in the design and conduct of the study; collection, management, analysis, and interpretation of the data; preparation, review, or approval of the manuscript; and decision to submit the manuscript for publication.

Additional Contributions: We thank the patients and their unaffected family members for their participation in this study. Elizabeth Hartnett scheduled the patient visits at the National Institutes of Health. Nigel Laing, PhD (Australian Neuromuscular Research Institute and Royal Perth Hospital), provided the vector for the cell transfections. No financial compensation was given for their services.

Correction: This article was corrected on July 9, 2015, to remove redundant information from the Discussion and to correct a reference.

REFERENCES

- Liewluck T, Tracy JA, Sorenson EJ, Engel AG. Scapulo-peroneal muscular dystrophy phenotype due to *TRIM32*-sarcotubular myopathy in South Dakota Hutterite. *Neuromuscul Disord*. 2013;23(2):133-138.
- Deng HX, Klein CJ, Yan J, et al. Scapulo-peroneal spinal muscular atrophy and CMT2C are allelic disorders caused by alterations in TRPV4. *Nat Genet*. 2010;42(2):165-169.
- Armstrong RM, Fogelson MH, Silberberg DH. Familial proximal spinal muscular atrophy. *Arch Neurol*. 1966;14(2):208-212.
- Goebel HH, Laing NG. Actinopathies and myosinopathies. *Brain Pathol*. 2009;19(3):516-522.
- Nowak KJ, Ravenscroft G, Laing NG. Skeletal muscle α -actin diseases (actinopathies): pathology and mechanisms. *Acta Neuropathol*. 2013;125(1):19-32.
- Schröder JM, Durling H, Laing N. Actin myopathy with nemaline bodies, intranuclear rods, and a heterozygous mutation in *ACTA1* (Asp154Asn). *Acta Neuropathol*. 2004;108(3):250-256.
- Sevdali M, Kumar V, Peckham M, Sparrow J. Human congenital myopathy actin mutants cause myopathy and alter Z-disc structure in *Drosophila* flight muscle. *Neuromuscul Disord*. 2013;23(3):243-255.
- Bromberg MB, Swoboda KJ. Motor unit number estimation in infants and children with spinal muscular atrophy. *Muscle Nerve*. 2002;25(3):445-447.
- Abecasis GR, Cherny SS, Cookson WO, Cardon LR. Merlin-rapid analysis of dense genetic maps using sparse gene flow trees. *Nat Genet*. 2002;30(1):97-101.
- Li H, Durbin R. Fast and accurate short read alignment with Burrows-Wheeler transform. *Bioinformatics*. 2009;25(14):1754-1760.
- McKenna A, Hanna M, Banks E, et al. The Genome Analysis Toolkit: a MapReduce framework for analyzing next-generation DNA sequencing data. *Genome Res*. 2010;20(9):1297-1303.
- DePristo MA, Banks E, Poplin R, et al. A framework for variation discovery and genotyping using next-generation DNA sequencing data. *Nat Genet*. 2011;43(5):491-498.
- Paavilainen VO, Oksanen E, Goldman A, Lappalainen P. Structure of the actin-depolymerizing factor homology domain in complex with actin. *J Cell Biol*. 2008;182(1):51-59.
- Brunger AT. Version 1.2 of the Crystallography and NMR system. *Nat Protoc*. 2007;2(11):2728-2733.
- Villefranc JA, Amigo J, Lawson ND. Gateway compatible vectors for analysis of gene function in the zebrafish. *Dev Dyn*. 2007;236(11):3077-3087.

16. Gupta V, Kawahara G, Gundry SR, et al. The zebrafish *dag1* mutant: a novel genetic model for dystroglycanopathies. *Hum Mol Genet.* 2011;20(9):1712-1725.
17. Costa CF, Rommelaere H, Waterschoot D, et al. Myopathy mutations in α -skeletal-muscle actin cause a range of molecular defects. *J Cell Sci.* 2004;117(pt 15):3367-3377.
18. McComas AJ, Sica RE, Upton AR. Multiple muscle analysis of motor units in muscular dystrophy. *Arch Neurol.* 1974;30(3):249-251.
19. Paganoni S, Amato A. Electrodiagnostic evaluation of myopathies. *Phys Med Rehabil Clin N Am.* 2013;24(1):193-207.
20. Sherry ST, Ward MH, Kholodov M, et al. dbSNP: the NCBI database of genetic variation. *Nucleic Acids Res.* 2001;29(1):308-311.
21. Nowak KJ, Wattanasirichaigoon D, Goebel HH, et al. Mutations in the skeletal muscle α -actin gene in patients with actin myopathy and nemaline myopathy. *Nat Genet.* 1999;23(2):208-212.
22. Laing NG, Clarke NF, Dye DE, et al. Actin mutations are one cause of congenital fibre type disproportion. *Ann Neurol.* 2004;56(5):689-694.
23. Agrawal PB, Strickland CD, Midgett C, et al. Heterogeneity of nemaline myopathy cases with skeletal muscle α -actin gene mutations. *Ann Neurol.* 2004;56(1):86-96.
24. Ilkovski B, Cooper ST, Nowak K, et al. Nemaline myopathy caused by mutations in the muscle α -skeletal-actin gene. *Am J Hum Genet.* 2001;68(6):1333-1343.
25. Kaindl AM, Rüschemdorf F, Krause S, et al. Missense mutations of *ACTA1* cause dominant congenital myopathy with cores. *J Med Genet.* 2004;41(11):842-848.
26. Jungbluth H, Sewry CA, Brown SC, et al. Mild phenotype of nemaline myopathy with sleep hypoventilation due to a mutation in the skeletal muscle α -actin (*ACTA1*) gene. *Neuromuscul Disord.* 2001;11(1):35-40.
27. Clarkson E, Costa CF, Machesky LM. Congenital myopathies: diseases of the actin cytoskeleton. *J Pathol.* 2004;204(4):407-417.
28. Feng JJ, Marston S. Genotype-phenotype correlations in *ACTA1* mutations that cause congenital myopathies. *Neuromuscul Disord.* 2009;19(1):6-16.
29. Figarella-Branger D, El-Dassouki M, Saenz A, et al. Myopathy with lobulated muscle fibers: evidence for heterogeneous etiology and clinical presentation. *Neuromuscul Disord.* 2002;12(1):4-12.
30. Weller B, Carpenter S, Lochmüller H, Karpati G. Myopathy with trabecular muscle fibers. *Neuromuscul Disord.* 1999;9(4):208-214.
31. Irodenko VS, Lee HS, de Armond SJ, Layzer RB. Adult nemaline myopathy with trabecular muscle fibers. *Muscle Nerve.* 2009;39(6):871-875.
32. Laing NG, Dye DE, Wallgren-Pettersson C, et al. Mutations and polymorphisms of the skeletal muscle α -actin gene (*ACTA1*). *Hum Mutat.* 2009;30(9):1267-1277.
33. Ilkovski B, Nowak KJ, Domazetovska A, et al. Evidence for a dominant-negative effect in *ACTA1* nemaline myopathy caused by abnormal folding, aggregation and altered polymerization of mutant actin isoforms. *Hum Mol Genet.* 2004;13(16):1727-1743.